Hawai'i: Their Life, Lore, and Environment (Bishop Museum, Honolulu, HI, 1972).
36. E. G. Jobbagy, R. B. Jackson, *Biogeochemistry* **53**, 51 (2001).
37. While mulching by Polynesian cultivators was not responsible for the presence of enriched soils within the field system, it could have contributed to the sharpness of the transition in soil properties from within the field system to just outside it (Fig. 3).
38. Although intensive agriculture expanded to the boundaries of suitable climates and soils in leeward Kohala, variation in the density of walls and trails suggests that the degree of agricultural intensification differed within the system (*17*).
39. O. A. Chadwick, L. A. Derry, P. M. Vitousek, B. J. Huebert, L. O. Hedin, *Nature* **397**, 491 (1999).
40. P. M. Vitousek, *Nutrient Cycling and Limitation: Hawai'i as a Model System* (Princeton Univ. Press, NJ, 2004).
41. P. V. Kirch *et al., Proc. Natl. Acad. Sci. U.S.A.*, in press.
42. O. A. Chadwick, unpublished data.
43. P. G. Murphy, A. E. Lugo, *Annu. Rev. Ecol. Syst.* **17**, 67 (1986).
44. J. J. Ewel, *Agrofor. Syst.* **45**, 1 (1999).
45. K. J. Willis, L. Gillson, T. M. Brncic, *Science* **304**, 402 (2004).
46. Supported by NSF grant BCS-0119819. We thank the State of Hawai'i for permission to carry out this research; Kahua, Parker, and Ponoholo Ranches and other Kohala landowners for access to their lands; D. Turner, S. Robinson, J. P. Fay, M. Vitousek, N. Boes, and V. Bullard for assistance with graphics and laboratory analyses; and J. Diamond and G. C. Daily for comments on an earlier draft of this manuscript.

Supporting Online Material
www.sciencemag.org/cgi/content/full/304/5677/1665/DC1
Materials and Methods
Figs. S1 to S5
Table S1
References

26 April 2004; accepted 14 May 2004

A Dual Role for *Hox* Genes in Limb Anterior-Posterior Asymmetry

József Zákány, Marie Kmita, Denis Duboule*

Anterior-to-posterior patterning, the process whereby our digits are differently shaped, is a key aspect of limb development. It depends on the localized expression in posterior limb bud of *Sonic hedgehog* (*Shh*) and the morphogenetic potential of its diffusing product. By using an inversion of and a large deficiency in the mouse *HoxD* cluster, we found that a perturbation in the early collinear expression of *Hoxd11*, *Hoxd12*, and *Hoxd13* in limb buds led to a loss of asymmetry. Ectopic *Hox* gene expression triggered abnormal *Shh* transcription, which in turn induced symmetrical expression of *Hox* genes in digits, thereby generating double posterior limbs. We conclude that early posterior restriction of *Hox* gene products sets up an anterior-posterior prepattern, which determines the localized activation of *Shh*. This signal is subsequently translated into digit morphological asymmetry by promoting the late expression of *Hoxd* genes, two collinear processes relying on opposite genomic topographies, upstream and downstream *Shh* signaling.

Anterior-posterior (AP) asymmetry in tetrapod limbs is reflected by the anatomy of lower arms and hands. In humans, the thumb is shorter and more mobile than other digits. These differences result from the presence in the developing posterior limb bud of a zone of polarizing activity (ZPA) (*1*), defined by its potential both to induce supernumerary digits and to modify digit identity when transplanted anteriorly. Cells within the ZPA express the *Shh* gene (*2*), whose product propagates posterior identity in the growing bud, likely through a graded, long-range intercellular signaling mechanism (*3*, *4*).

The effects of *Shh* signaling in limbs are mediated, at least in part, by posterior *Hoxd* genes (*2*, *5*–*9*) because of the potential of SHH to prevent the production of the repressor form of GLI3 protein, which negatively regulates *Hox* gene transcription (*10*–*12*), likely through a global digit enhancer located near the *HoxD* cluster (*13*, *14*). Models for the restriction of *Shh* expression in posterior limb bud cells have been proposed whereby the antagonism between the *Gli3* and *dHand* transcription factors would initially divide the bud into anterior and posterior domains (*15*). Although this model is supported by genetics and experimental data (*11*, *12*, *16*–*18*), it falls short in explaining the spatial restriction of *Shh* expression.

A similar limb bud posterior specificity was observed for both *Hoxa* and *Hoxd* genes in their earliest phases of expression (*19*–*21*). *Hoxd* genes are activated in a collinear fashion, with *Hoxd1* and *Hoxd3* expressed throughout the early bud, whereas *Hoxd12* and *Hoxd13* are expressed posteriorly (Fig. 1A) in a domain containing future SHH-positive cells. This restriction occurs before *Shh* expression (*5*, *6*, *9*, *22*), which suggested a role for *Hox* genes in AP polarity (*19*). In addition, ectopic expression of *Hoxb8* and *Hoxd12* revealed the potential of some HOX products to trigger *Shh* expression (*23*–*25*). Here, we use two novel genomic rearrangements to show that posterior *Hoxd* genes are key determinants in the early organization of limb AP asymmetry.

We engineered a *loxP*/Cre-dependent inversion of the *HoxD* cluster (Fig. 1A) and asked whether gene expression would be con-

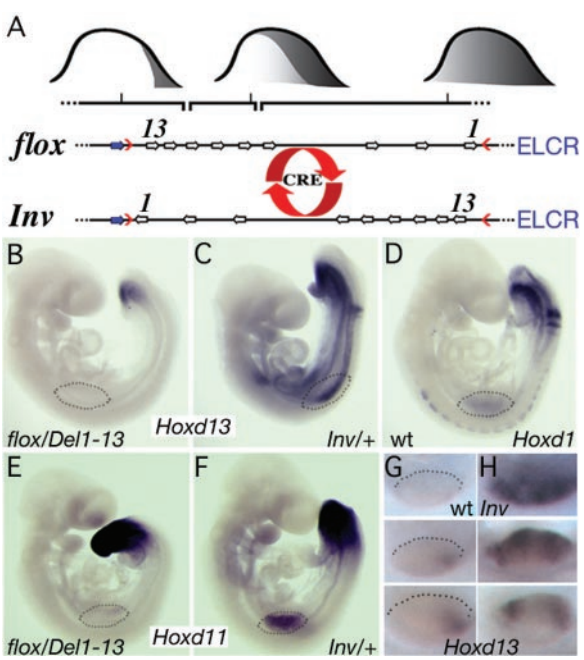

Fig. 1. Targeted inversion of the *HoxD* cluster. (**A**) Collinear expression patterns (in gray) of *Hoxd* genes in limb bud. The *HoxD* cluster is shown with blue arrows for a *Hoxd11lac* reporter gene (*27*) and white block arrows for *Hoxd* genes. Red arrowheads are *loxP* sites. The presence of an ELCR is shown in blue. The *loxP*/Cre conditional inversion allele is also shown. Exposure to the Cre recombinase in vitro (red arrows) generated both *flox* and *Inv* alleles. (**B**) Control *Hoxd13* expression (one copy) in an E9.5 embryo. (**C**) *Hoxd13* expression in a de novo isolated (*28*) (Materials and Methods) *Inv*/+ embryo, showing an anterior shift in expression including the forelimb field (dotted lines), similar to *Hoxd1* (**D**). *Hoxd11* expression in E9 embryo with one copy (**E**) or *Inv*/+ embryo (**F**). *Hoxd13* staining in forelimb buds of normal (**G**) and *Inv* chimeric (**H**) embryos. The expected posterior pattern is seen in the larger two specimens [(G), bottom], whereas chimeras show premature expression in the entire bud (H).

Department of Zoology and Animal Biology and National Program Frontiers in Genetics, University of Geneva, Sciences III, Quai Ernest Ansermet 30, 1211 Geneva 4, Switzerland.

*To whom correspondence should be addressed. E-mail: Denis.Duboule@zoo.unige.ch

comitantly modified. Because embryos carrying the inversion (*Inv*) did not survive, we induced the inversion in vivo, along with a wild-type chromosome, or analyzed mosaic fetuses containing both the *Inv* and the non-inverted alleles after recombination in vitro. When the *Inv* allele was present, expression of both *Hoxd13* (Fig. 1, C, G, and H, and fig. S1) and *Hoxd11* (Fig. 1F) was seen in the anterior domain. Expression of *Hoxd1* is shown in Fig. 1D as a control. Expression of a single copy of *Hoxd13* (Fig. 1B) and *Hoxd11* (Fig. 1E) using the floxed configuration over a deletion of the *HoxD* cluster (*flox/Del1-13*) showed no anterior ectopic expression. We concluded that, on inversion, *Hoxd13* and *Hoxd11* had been brought to the vicinity of an early limb control region (ELCR) (Fig. 1), located telomeric to *HoxD*, that normally drives expression throughout limb bud cells.

To ascertain both the existence and the location of an ELCR, we analyzed a deletion of *Hoxd1* to *Hoxd10* obtained by targeted meiotic recombination (fig. S2A) [*Del(1-10)*]. This deficiency generated a minicluster composed of *Hoxd11*, *Hoxd12*, and *Hoxd13*, now located as close to a potential ELCR as in the inversion but in their native orientation and genomic order (Fig. 2A). Homozygous *Del1-10* mice died soon after birth; hence specimens were analyzed either as fetuses or newborns. Homozygous newborns showed a markedly elongated thumb in forelimbs (Fig. 2, B and E, asterisks), making the AP asymmetry hardly recognizable. Furthermore, homozygotes displayed a perfectly symmetrical carpus, with bones organized in a mirror image (Fig. 2E), and the distal radius acquired the morphology of distal ulna. This bilateral symmetry, seen in the right limbs of eight animals, occurred less frequently in the corresponding left limbs. In addition, three homozygous animals had only four digits in their forelimbs (Fig. 2C), and hindlimb polydactyly was scored in both homozygous and heterozygous individuals. In all cases, digits appeared organized following a mirror symmetry, as exemplified by an additional large palmar cushion at the base of the most anterior digit (Fig. 2G).

The loss of AP asymmetry suggested that the deletion had modified the expression of the remaining *Hoxd* genes. *Hoxd13* expression (Fig. 3A) was detected at high amounts in both heterozygous and homozygous animals. However, contrary to what is seen in wild-type mice, *Hoxd13* was scored in anterior cells of homozygous mice at day 11 of the embryo (E11) within the digits as well as along the anterior circumference of the limb, including both lower and upper arm primordia (Fig. 3B). Consequently, *Hoxd13* transcript pattern in homozygous limbs was no longer skewed posteriorly. Therefore, symmetrical expression of *Hox* genes coincided with double-posterior hand plates. At E10, *Hoxd13*-expressing cells are normally located distal and posterior (Fig. 3C). In heterozygotes, two additional domains located at the anterior and posterior base of the bud ex-

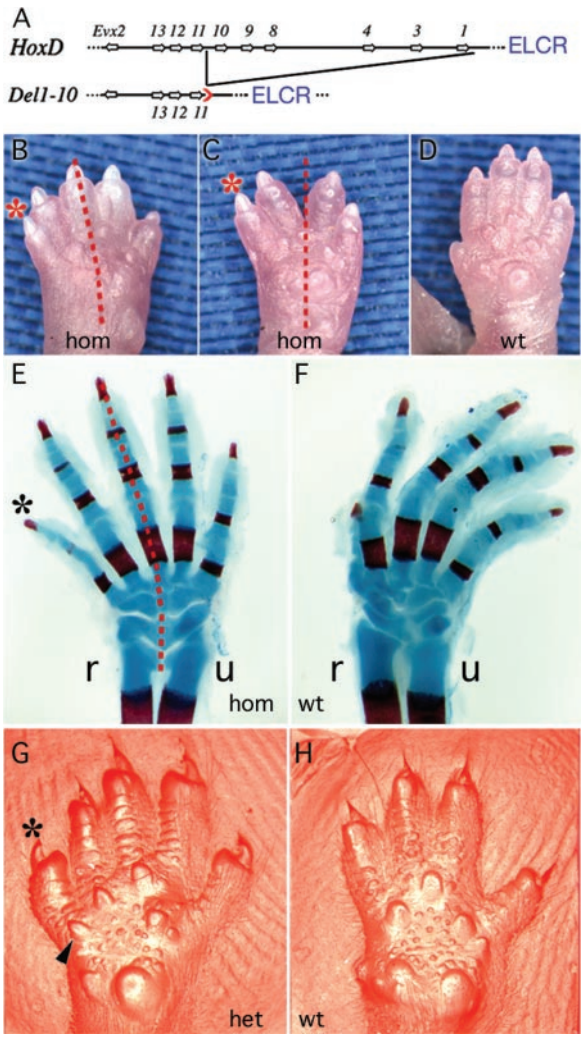

Fig. 2. A mini *HoxD* cluster. (**A**) Derivation of the *Del1-10* allele by meiotic recombination (*28–31*) (Materials and Methods). Symbols are as in Fig. 1A. Forelimb paws of homozygous (hom) mutant [(**B**) and (**C**)] and wild-type (wt) (**D**) newborns. Bone (red) and cartilage (blue) pattern of newborn homozygous mutant (**E**) and wild-type (**F**) autopods. r, radius; u, ulna. Palm clay prints of a heterozygous (het) mutant (**G**) and a normal (**H**) adult animal. Asterisks point to the elongated digit I. The supernumerary anterior cushion is shown with arrowhead. The red dotted lines indicate the plane of AP mirror symmetry.

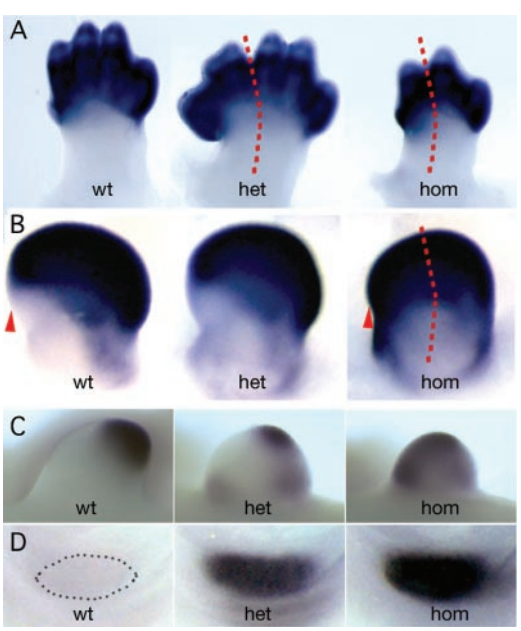

Fig. 3. *Hoxd13* expression in *Del1-10* embryos. Homozygous, heterozygous, and wild-type littermates are compared. Expression of *Hoxd13* at E13 (**A**), E11 (**B**), E10 (**C**), and E9 (**D**) shows loss of asymmetry (arrowhead indicates presumptive digit I). Anterior regions displayed ectopic *Hoxd13* signal, and a mirror image pattern was visible in all homozygous and some heterozygous specimens. Whereas at E9, both *Hoxd11* and *Hoxd13* were expressed throughout the bud (D), this ectopic domain was not maintained and appeared as two weak patches located proximally at E10 (C). At this latter stage, the wild-type domain appeared distally, though with an unusual central position [(C), middle and right]. Red and black dotted lines indicate the plane of AP symmetry and limb bud field, respectively.

pressed *Hoxd13*. At E9.5, homozygous limbs displayed an even more homogenous signal, because we detected *Hoxd13* and *Hoxd11* transcripts throughout the limb buds (Fig. 3D), supporting the presence of an ELCR 3′ of *Hoxd1*. All three posterior genes showed similar misregulation (fig. S3).

This latter ectopic expression nevertheless rapidly subsided and thus could not account for the subsequent symmetrical *Hox* profiles in digits. Because *Hox* expression in digits is likely under the control of *Shh* signaling, we looked at *Shh* transcripts in these mutant buds. In limbs of early and late E9.5 wild-type embryos, *Shh* transcripts were restricted to a posterior spot (Fig. 4, A and B). By E10, this positive domain had extended while remaining posterior and shifting distally (Fig. 4C), and by E10.5 transcript accumulated within the posterior half (Fig. 4D). *Del1-10* homozygous embryos showed clusters of ectopic *Shh*-expressing cells, either as an extension of the normal domain anteriorly and distally (Fig. 4, E and F) or along the anterior edge (Fig. 4G), leading in some cases to mirror-image domains (Fig. 4H). In these buds, the expression profiles of the *Gli3* and *dHand* genes were modified concomitantly (fig. S3). Therefore, ectopic posterior *Hox* products in early anterior buds were sufficient to trigger *Shh* transcription in cells that eventually established an ectopic *Shh* anterior domain, suggesting that *Shh* expression is normally controlled by posterior *Hox* genes.

In these experiments, we did not observe mirror-image duplications with polydactyly, as seen with ZPA grafts where a similar amount of ectopic SHH was present. We think this is because of the absence of many *Hoxd* genes and the observed down-regulation of *Hoxd11* in digits (fig. S2, B and C). *Hox* genes are required for proper growth of the appendages, and their absence prevented mutant buds from fully developing a duplicated pattern because of an initial size reduction. Full mirror-image duplications obtained with SHH, ZPA grafts, or retinoid treatment are thus likely *Hox*-dependent. Supernumerary digits in forelimbs were only scored in heterozygotes containing a complete set of *Hoxd* genes, which supports this view.

The mechanism progressively restricting *Hox* gene transcription to posterior limb bud cells is crucial for the limb AP asymmetry by triggering localized *Shh* transcription. Although the underlying process is elusive, both the inverted and deleted configurations reported here suggest that a regulatory sequence localized telomeric to the cluster (ELCR) (Fig. 5) is needed to implement this collinear regulation. Because *Hoxd* promoters equally respond to this ELCR when located nearby, a distance effect may progressively prevent anterior cells from transcribing genes located far from the ELCR. Once activated posteriorly, *Shh* will subsequently control *Hoxd* gene transcription in presumptive digits with the use of another collinear strategy (*14*), likely mediated by an enhancer located centromeric to the cluster [global center region (GCR)] (*13*). In early limb development, 5′-located *Hoxd* genes are repressed in anterior cells, probably by the GLI3 repressor protein (*26*). By contrast, in the late phase, the same genes are heavily, but unequally, transcribed in most distal cells because of an opposite distance effect whereby posterior *Hoxd* genes preferentially respond to the GCR sequence (*14*). In this view, *Shh* signaling acts as a relay mechanism between two "opposite" collinear strategies to translate an initial molecular asymmetry into its morphological readout, digit identities.

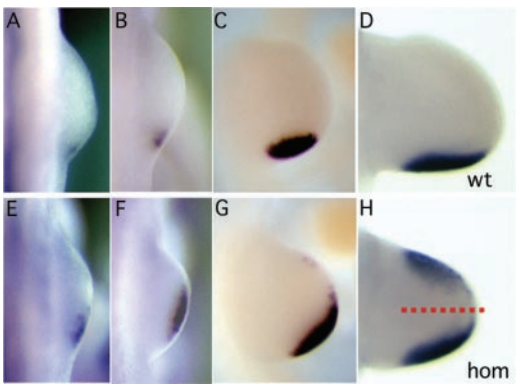

Fig. 4. *Shh* expression in mutant limb buds. Wild-type embryos at E9.5 [(**A**) and (**B**)], E10 (**C**), and E10.5 (**D**). *Shh* expression in *Del1-10* mutants at E9.5 [(**E**) and (**F**)], E10 (**G**), and E10.5 (**H**). Ectopic *Shh* expression in early buds was systematically scored [compare (A) to (E) and (B) to (F)]. The normal *Shh* profile (B) was lost, and a larger, more distally located domain was observed (F). Subsequently, this domain was preferentially reinforced and maintained at both margins of the growing limb [(G) and (H)]. Note the scattered anterior signal, which could be observed (G), and the robust ectopic domain seen only in homozygotes (H).

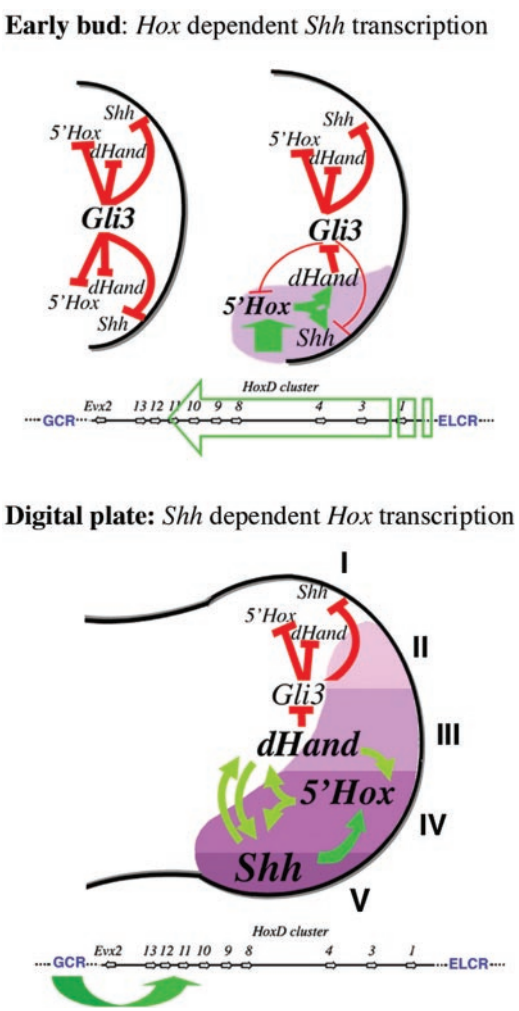

Fig. 5. Model for the onset of limb AP asymmetry. Red bars and green arrows indicate negative and positive effects, respectively. Anterior is on top. In the early bud phase (**top**), *Gli3* is expressed without AP asymmetry. The repressor form (GLI3R) (*10*) is present throughout the bud, suppressing transcription of posterior *Hoxd* genes *Shh* and *dHand* (*11*, *12*). *Hox* gene collinear activation leads to specific accumulation of group 10 to 13 transcripts posteriorly, perhaps as a distance effect from the ELCR (top, purple domain). These latter products trigger expression of *Shh* and *dHand*, which activate each other and limit the level of GLI3R accumulation posteriorly, either by inhibiting GLI3-to-GLI3R protein conversion (*12*) or by directly suppressing *Gli* transcription (*15*). Subsequently (**bottom**), in the posterior part, positive feedback loops between *5′Hox* genes, *Shh*, and *dHand* trigger the progressive expansion of this posterior identity (*2*, *16*, *17*), mostly through the graded impact of the SHH product on *Hox* gene expression in the distal bud (*32*), a process presumably under the control of the GCR (*13*). I to V indicate presumptive digits, and the graded pink zones represent the SHH gradient.

References and Notes

1. C. Tickle, *Int. J. Dev. Biol.* **46**, 847 (2002).
2. R. D. Riddle, R. L. Johnson, E. Laufer, C. Tabin, *Cell* **75**, 1401 (1993).
3. R. Dillon, C. Gadgil, H. G. Othmer, *Proc. Natl. Acad. Sci. U.S.A.* **100**, 10152 (2003).

4. G. Drossopoulou *et al*., *Development* **127**, 1337 (2000).
5. M. A. Ros *et al*., *Development* **130**, 527 (2003).
6. P. Kraus, D. Fraidenraich, C. A. Loomis, *Mech. Dev.* **100**, 45 (2001).
7. J. Sharpe *et al.*, *Curr. Biol.* **9**, 97 (1999).
8. H. Masuya, T. Sagai, S. Wakana, K. Moriwaki, T. Shiroishi, *Genes Dev.* **9**, 1645 (1995).
9. C. J. Neumann, H. Grandel, W. Gaffield, S. Schulte-Merker, C. Nusslein-Volhard, *Development* **126**, 4817 (1999).
10. B. Wang, J. F. Fallon, P. A. Beachy, *Cell* **100**, 423 (2000).
11. P. te Welscher *et al*., *Science* **298**, 827 (2002).
12. Y. Litingtung, R. D. Dahn, Y. Li, J. F. Fallon, C. Chiang, *Nature* **418**, 979 (2002).
13. F. Spitz, F. Gonzalez, D. Duboule, *Cell* **113**, 405 (2003).
14. M. Kmita, N. Fraudeau, Y. Herault, D. Duboule, *Nature* **420**, 145 (2002).
15. P. te Welscher, M. Fernandez-Teran, M. A. Ros, R. Zeller, *Genes Dev.* **16**, 421 (2002).
16. J. Charite, D. G. McFadden, E. N. Olson, *Development* **127**, 2461 (2000).
17. M. Fernandez-Teran *et al*., *Development* **127**, 2133 (2000).
18. D. Buscher, B. Bosse, J. Heymer, U. Ruther, *Mech. Dev.* **62**, 175 (1997).
19. P. Dolle, J. C. Izpisua-Belmonte, H. Falkenstein, A. Renucci, D. Duboule, *Nature* **342**, 767 (1989).
20. H. Haack, P. Gruss, *Dev. Biol.* **157**, 410 (1993).
21. C. E. Nelson *et al*., *Development* **122**, 1449 (1996).
22. U. Grieshammer, G. Minowada, J. M. Pisenti, U. K. Abbott, G. R. Martin, *Development* **122**, 3851 (1996).
23. J. Charite, W. de Graaff, S. Shen, J. Deschamps, *Cell* **78**, 589 (1994).
24. V. Knezevic *et al*., *Development* **124**, 4523 (1997).
25. S. Mackem, V. Knezevic, *Cell Tissue Res.* **296**, 27 (1999).
26. A. Zuniga, R. Zeller, *Development* **126**, 13 (1999).
27. F. van der Hoeven, J. Zakany, D. Duboule, *Cell* **85**, 1025 (1996).
28. F. Vidal, J. Sage, F. Cuzin, M. Rassoulzadegan, *Mol. Reprod. Dev.* **51**, 274 (1998).
29. Y. Herault, M. Rassoulzadegan, F. Cuzin, D. Duboule, *Nat. Genet.* **20**, 381 (1998).
30. J. Zakany, M. Kmita, P. Alarcon, J. L. de la Pompa, D. Duboule, *Cell* **106**, 207 (2001).
31. J. Zakany, M. Gerard, B. Favier, D. Duboule, *EMBO J.* **16**, 4393 (1997).
32. P. M. Lewis *et al*., *Cell* **105**, 599 (2001).
33. We thank M. Friedli and N. Fraudeau for technical assistance; J. Deschamps, C. Tabin, J. Cobb, and P. Vassalli for comments; and J. Deschamps, A. Zuniga, D. Srivastava, and A. McMahon for probes. This work was supported by funds from the Canton de Genève, the Swiss National Research Fund, the Claraz and Louis-Jeantet foundations and European Union grants "Eumorphia" and "Cells into Organs."

Supporting Online Material
www.sciencemag.org/cgi/content/full/304/5677/1669/DC1
Materials and Methods
Figs. S1 to S3

26 January 2004; accepted 7 April 2004

Phosphoryl Transfer and Calcium Ion Occlusion in the Calcium Pump

Thomas Lykke-Møller Sørensen,[1] Jesper Vuust Møller,[2]* Poul Nissen[1]*

A tight coupling between adenosine triphosphate (ATP) hydrolysis and vectorial ion transport has to be maintained by ATP-consuming ion pumps. We report two crystal structures of Ca^{2+}-bound sarco(endo)plasmic reticulum Ca^{2+}–adenosine triphosphatase (SERCA) at 2.6 and 2.9 angstrom resolution in complex with (i) a nonhydrolyzable ATP analog [adenosine (β–γ methylene)–triphosphate] and (ii) adenosine diphosphate plus aluminum fluoride. SERCA reacts with ATP by an associative mechanism mediated by two Mg^{2+} ions to form an aspartyl-phosphorylated intermediate state (Ca_2-E1∼P). The conformational changes that accompany the reaction with ATP pull the transmembrane helices 1 and 2 and close a cytosolic entrance for Ca^{2+}, thereby preventing backflow before Ca^{2+} is released on the other side of the membrane.

The electrochemical gradients for cations across biomembranes are maintained by P-type adenosine triphosphatases (ATPases), also known as cation pumps, that use energy derived from ATP to transport cations (*1*, *2*). Active transport by P-type ATPases is dependent on the formation of a covalent aspartyl-phosphoanhydride intermediate with ATP. Prominent P-type ATPases include Na^+,K^+-ATPases and fungal/plant H^+-ATPases that pump Na^+ and H^+, respectively, thereby controlling the intracellular environment, the membrane potential, and the ability to perform secondary transport. In skeletal muscle, the dominant P-type ATPase is sarco(endo)plasmic reticulum Ca^{2+}-ATPase (SERCA), which is responsible for the re-uptake into the sarcoplasmic reticulum of cytosolic Ca^{2+} released during muscle contraction; lowering cytosolic Ca^{2+} shuts down the activity of the myosin-actin filaments (*3*, *4*). Together with plasma membrane Ca^{2+}-ATPases, SERCA is also involved in signal transduction pathways that use intracellular Ca^{2+} as a second messenger.

The energy released by hydrolysis of ATP makes possible the uptake of cytoplasmic cation at a low concentration and its release on the other side of the membrane at a higher concentration. A central event in the functional cycle of P-type ATPases is the formation of a high-energy aspartyl-phosphoanhydride intermediate by reaction with ATP (E1-ATP → E1∼P), which primes a downhill transition to a low-energy E2-P state coupled to the uphill translocation of bound cation from the cytosol side in the E1∼P state to the other side of the membrane in the E2-P state. Kinetic data demonstrate that formation of the high-energy phosphorylated intermediate, including complexes with adenosine diphosphate and aluminum fluoride ($ADP:AlF_4^-$) or chromium ATP as transition-state mimics, is coupled to occlusion of the intramembraneously bound cations as exemplified by SERCA (*5*–*10*). Unprofitable backflow to the cytosol and uncoupled ATPase activity are thus prevented (*1*, *11*). This coupling of hydrolytic and vectorial processes is a key functional requirement of the cation pumps. The P-type cation pumps are part of the haloacid dehalogenase (HAD) superfamily, which displays a common fold and a set of conserved active-site residues including the phosphorylated aspartic acid side chain of P-type ATPases (*12*).

The crystal structures of SERCA from rabbit fast-twitch muscle in a nucleotide-free, Ca^{2+}-bound E1 (Ca_2-E1) state (*13*) and in an inhibitor-stabilized Ca^{2+}-free E2-thapsigargin state (*14*) represent a milestone in the study of ion pumps. They have confirmed in atomic detail the presence of ten (M1 through M10) transmembrane helices (*15*) and three cytoplasmic domains: an A ("actuator" or "anchor") domain, a P ("phosphorylation") domain, and an N ("nucleotide-binding") domain. The coordination of two Ca^{2+} ions at the center of the membrane-spanning region is in accordance with previous mutation data (*16*, *17*). Whereas the E2 state is compact, in accordance with the structure of decavanadate stabilized ATPase in two-dimensional crystals (*18*), in the Ca_2-E1 crystals the cytoplasmic domains adopt an open arrangement with no evident relation between the N domain and the phosphorylation site (Asp^{351}) in the P domain. Although studies of related proteins of the HAD superfamily provide a putative phosphorylation mechanism for P-type ATPases (*12*, *19*), the open structure of Ca_2-E1 poses unsolved questions on the structural basis of ATP binding, and the phosphoryl transfer reaction coupled to Ca^{2+} occlusion in the E1-P state in Ca^{2+}-ATPase remains elusive.

We crystallized rabbit fast-twitch muscle SERCA as Ca_2-E1–adenosine (β–γ methylene)–triphosphate (AMPPCP) and Ca_2-E1-$ADP:AlF_4^-$ complexes by the vapor-diffusion method after solubilization with $C_{12}E_8$ and in the presence of native lipids (*20*). The two

[1]Department of Molecular Biology, University of Aarhus, Gustav Wieds Vej 10C, DK-8000 Aarhus C, Denmark. [2]Department of Biophysics, University of Aarhus, Ole Worms Allé 185, DK-8000 Aarhus C, Denmark.

*To whom correspondence should be addressed. E-mail: jvm@biophys.au.dk (J.V.M.) and nissen@imsb.au.dk (P.N.)